



American Society of Hematology
 2021 L Street NW, Suite 900,
 Washington, DC 20036
 Phone: 202-776-0544 | Fax 202-776-0545
 editorial@hematology.org

Human genetic defects in SRP19 and SRPRA cause severe congenital neutropenia with distinctive proteome changes

Tracking no: BLD-2022-016783R2

Monika Linder (Ludwig-Maximilians-Universität München, Germany) Yoko Mizoguchi (Dr. von Hauner Children's Hospital, University Hospital, LMU, Germany) Sebastian Hesse (Dr. von Hauner Children's Hospital, LMU Klinikum, Germany) Gergely Csaba (Institute of Bioinformatics, Germany) Megumi Tatematsu (Dr. von Hauner Children's Hospital, LMU Klinikum, Germany) Marcin Łyszczewicz (Dr. von Hauner Children's Hospital, University Hospital, LMU, Germany) Natalia Zietara (Dr. von Hauner Children's Hospital, University Hospital, LMU, Germany) Tim Jeske (Department of Pediatrics, Dr. von Hauner Children's Hospital, University Hospital, LMU Munich, Germany) Maximilian Hastreiter (Ludwig-Maximilians-Universität München, Germany) Meino Rohlf (Dr. von Hauner Children's Hospital, Department of Pediatrics, University Hospital, LMU Munich,) Yanshan Liu (Ludwig-Maximilians-Universität München, Germany) Piotr Grabowski (TU Berlin, Germany) Kaarin Ahomaa (Institute of Bioinformatics and Systems Biology, Germany) Daniela Maier-Begandt (Ludwig-Maximilians-Universität München, Germany) Marko Schwestka (Australian Regenerative Medicine Institute, Australia) Vahid Pazhakh (Monash University, Australia) Abdulsalam Isiaku (Australian Regenerative Medicine Institute, Australia) Brenda Briones Miranda (Australian Regenerative Medicine Institute, Australia) Piers Blombery (Peter MacCallum Cancer Centre, Australia) Megumu Saito (Kyoto university, Japan) Ejona Rusha (Induced Pluripotent Stem Cell Facility, Germany) Zahra Alizadeh (Immunology, Asthma and Allergy Research Institute, Iran, Islamic Republic of) Zahra Pourpak (Immunology, Asthma & Allergy Research Institute, Tehran University of Medical Sciences, Iran, Islamic Republic of) Masao Kobayashi (Hiroshima University Graduate School of biomedical Sciences, Japan) Nima Rezaei (Tehran University of Medical Sciences, Iran, Islamic Republic of) Ekrem Unal (Erciyes University, Pediatric Hematology Oncology, Turkey) Fabian Hauck (Dr. von Hauner Children's Hospital, Ludwig-Maximilians-Universität, Germany) Micha Drukker (Helmholtz Center Munich, Germany) Barbara Walzog (Ludwig-Maximilians-Universität, Germany) Juri Rappsilber (Technische Universität Berlin; Wellcome Centre for Cell Biology, University of Edinburgh,) Ralf Zimmer (Ludwig-Maximilians-Universität München, Germany) Graham Lieschke (Australian Regenerative Medicine Institute, Australia) Christoph Klein (Dr. von Hauner Children's Hospital, LMU Klinikum, Germany)

Abstract:

The mechanisms of coordinated changes in proteome composition and their relevance for the differentiation of neutrophil granulocytes are not well studied. Here, we discover two novel human genetic defects in SRPRA and SRP19, constituents of the mammalian co-translational targeting machinery and characterize their role in neutrophil granulocyte differentiation. We systematically study the proteome of neutrophil granulocytes from patients with variants in the signal recognition particle (SRP) genes, HAX1, and ELANE and identify global as well as specific proteome aberrations. Using *in vitro* differentiation of human induced pluripotent stem cells and *in vivo* zebrafish models, we study the effects of SRP-deficiency on neutrophil granulocyte development. In a heterologous cell-based inducible protein expression system, we validate the effects conferred by SRP dysfunction for selected proteins that we identified in our proteome screen. Thus, SRP-dependent protein processing, intracellular trafficking and homeostasis are critically important for the differentiation of neutrophil granulocytes.

Conflict of interest: No COI declared

COI notes:

Preprint server: No;

Author contributions and disclosures: Original idea: C.K.; Conceptualization and Methodology: C.K. M.I.L. Y.M., S.H., R.Z.; Clinical and patient-related investigations: C.K., S.H., A.Z., M.K., N.R., E.Ü., F.H.; Experimentation: M.I.L., Y.M., S.H., M.T., N.Z., M.R., Y.L., P.G., D.M., M.S., E.R., M.D.; M.S.; A.I.I., B.B.M.; Computational analysis: S.H., G.C., A.K., T.J., M.H., R.Z.; Resources: M.D., B.W., J.R., R.Z., C.K.; P.B., G.J.L.; Data Curation: C.G., R.M. R.Z.; M.S.; Writing Original Drafts: C.K., M.I.L., S.H., Y.M.; G.J.L.; Supervision: C.K., B.W., V.P., R.Z., J.R.; G.J.L.; Writing, Review & Editing of draft, all authors;

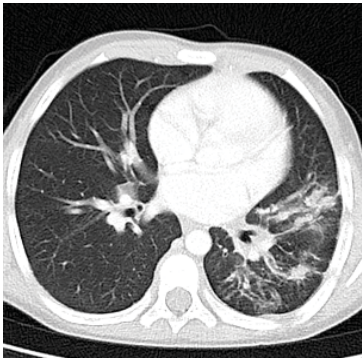
Non-author contributions and disclosures: No;

Agreement to Share Publication-Related Data and Data Sharing Statement: Will be included once manuscript is accepted.

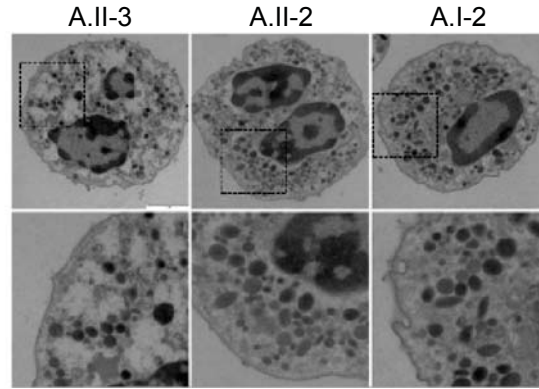
Clinical trial registration information (if any):

Figure 1

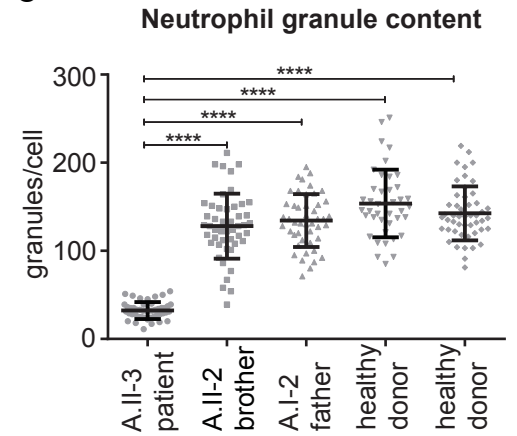
A



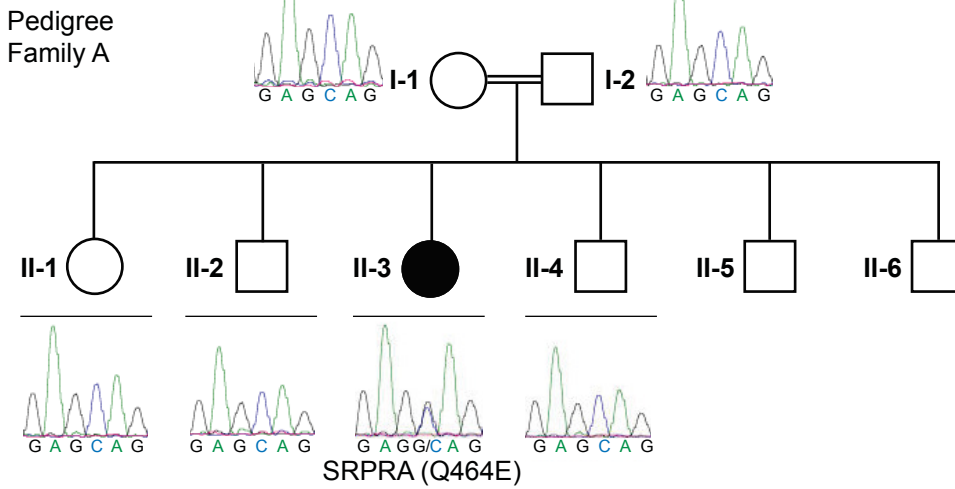
B



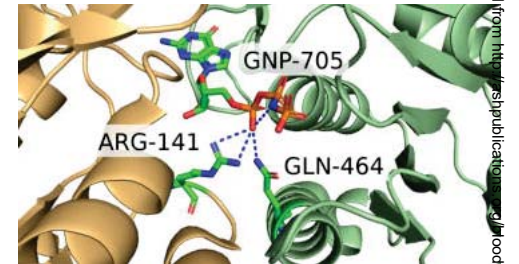
C



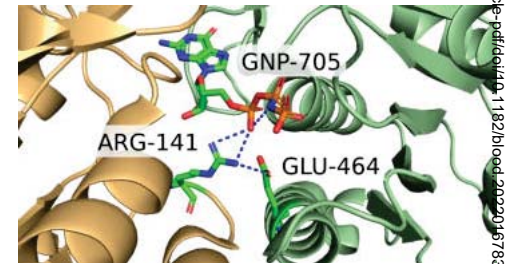
D



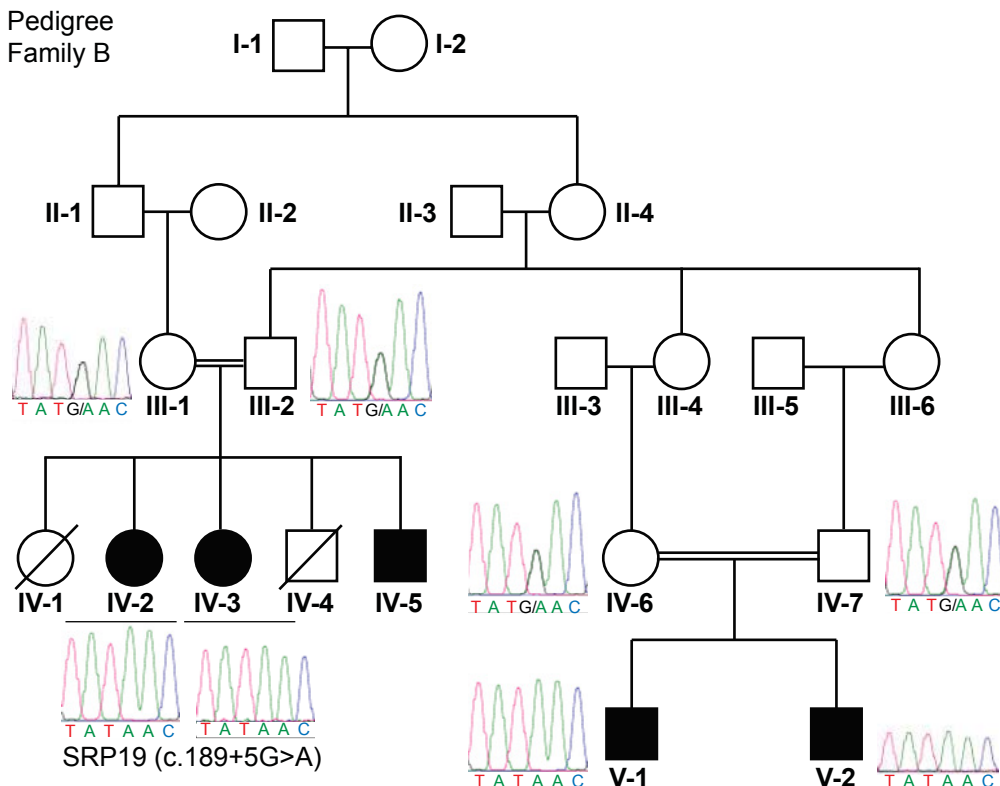
E



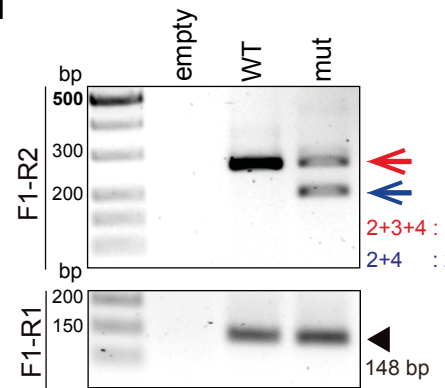
F



G



H



I

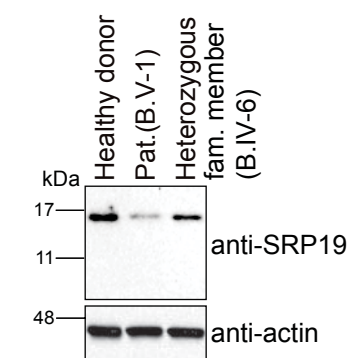
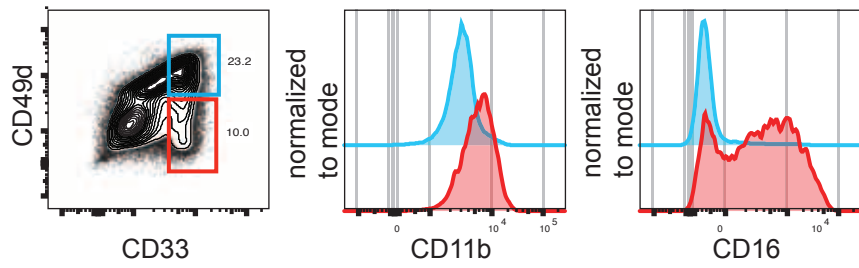
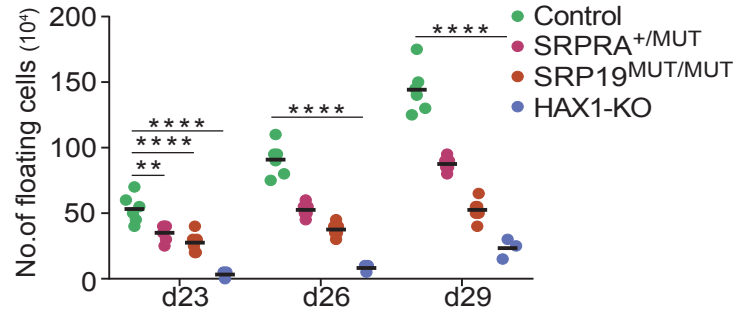


Figure 2

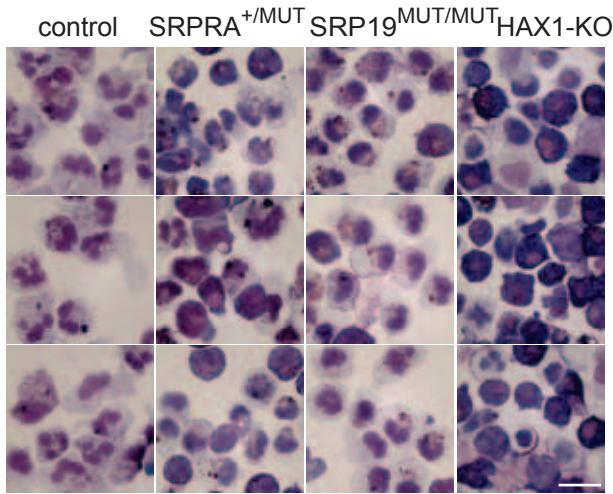
A



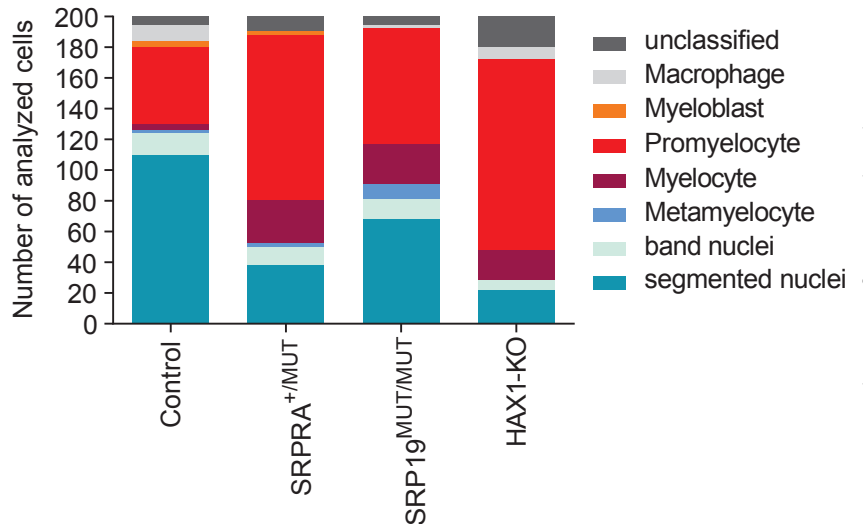
B



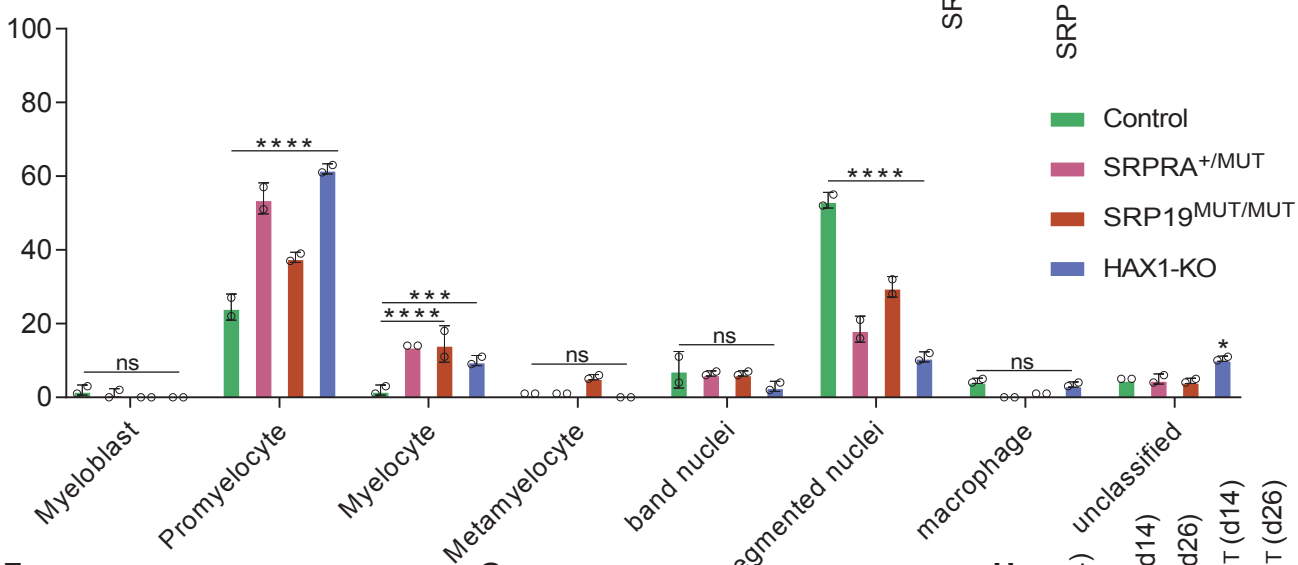
C



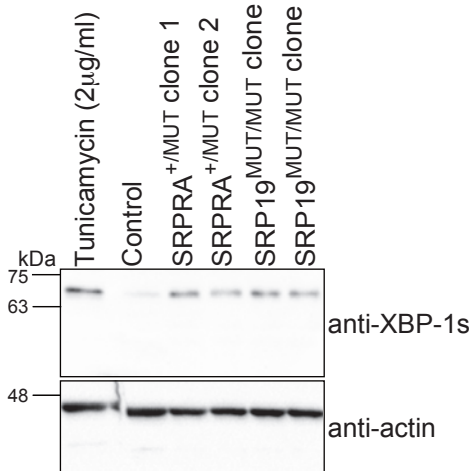
D



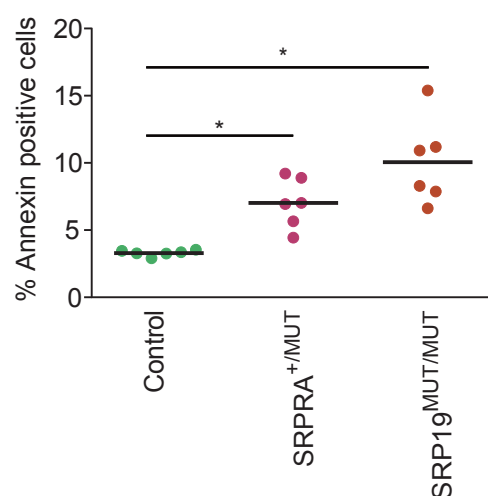
E



F



G



H

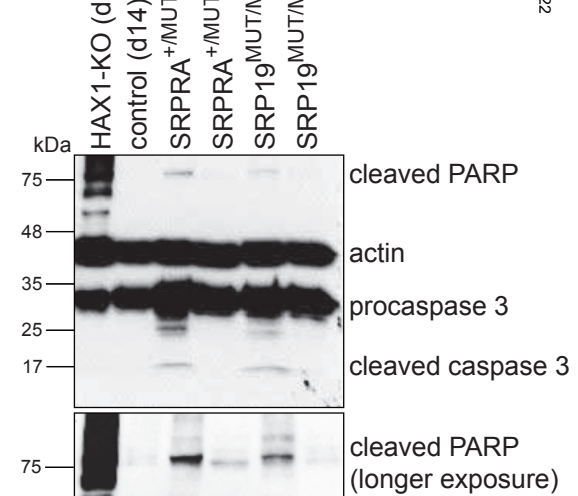


Figure 3

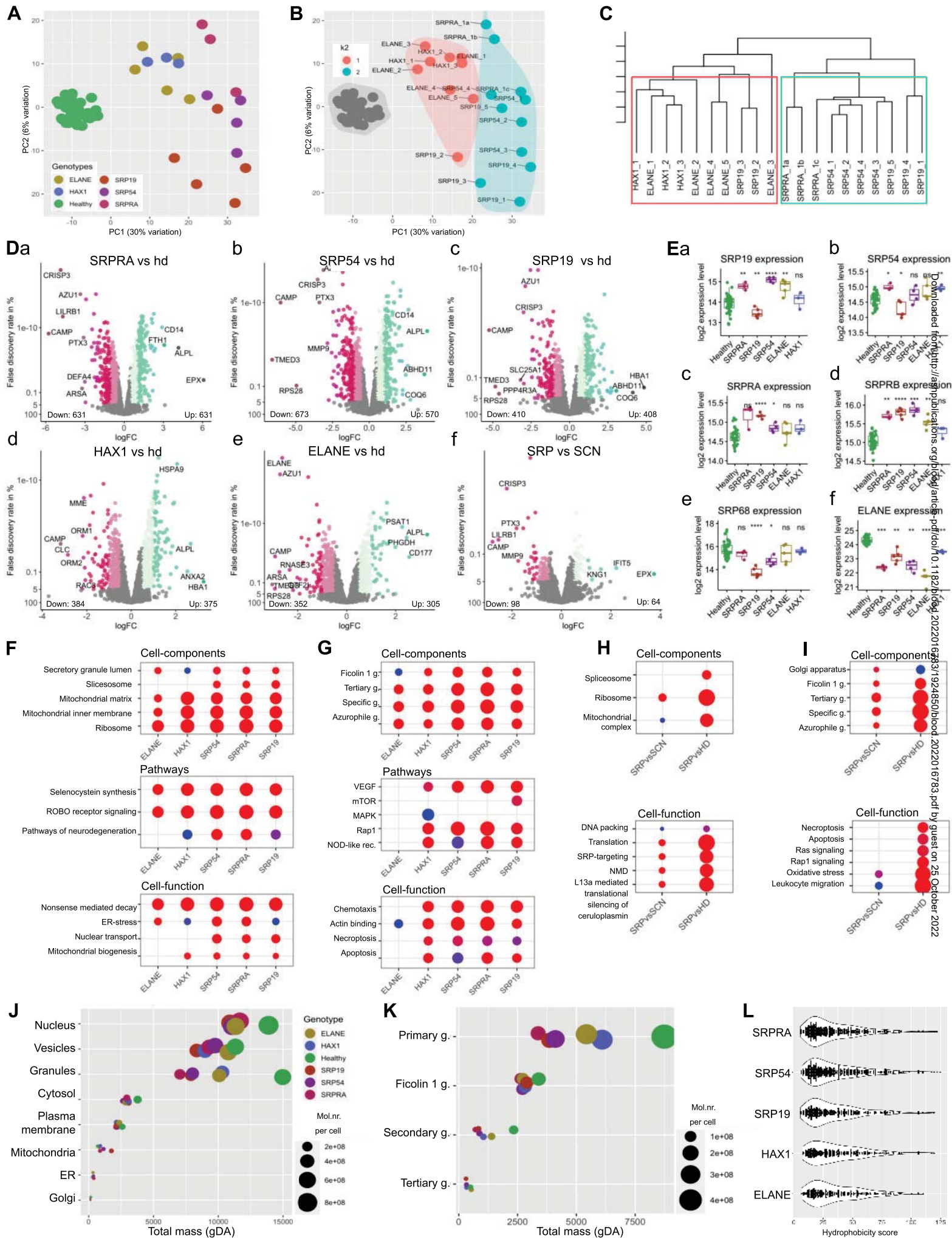


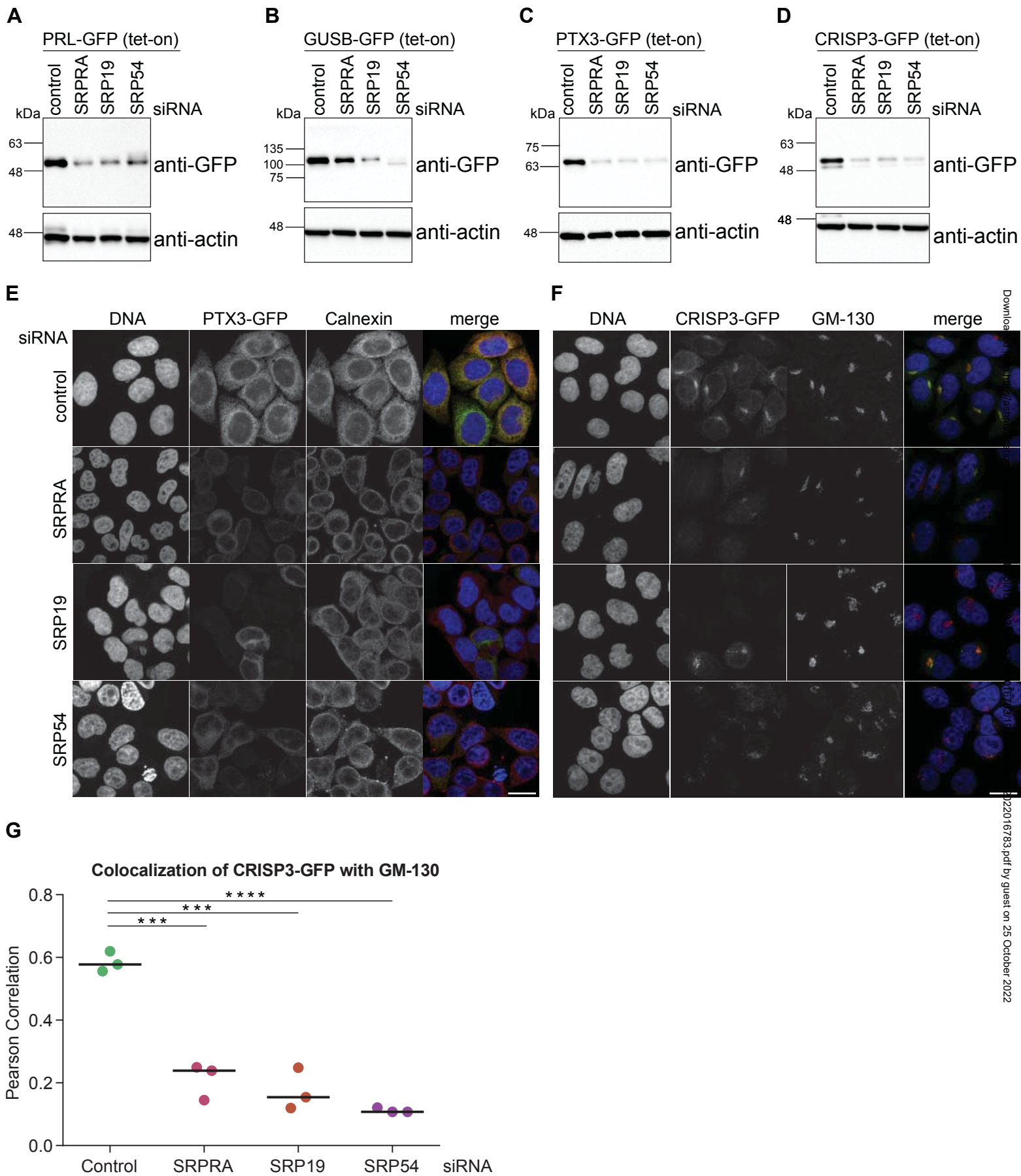
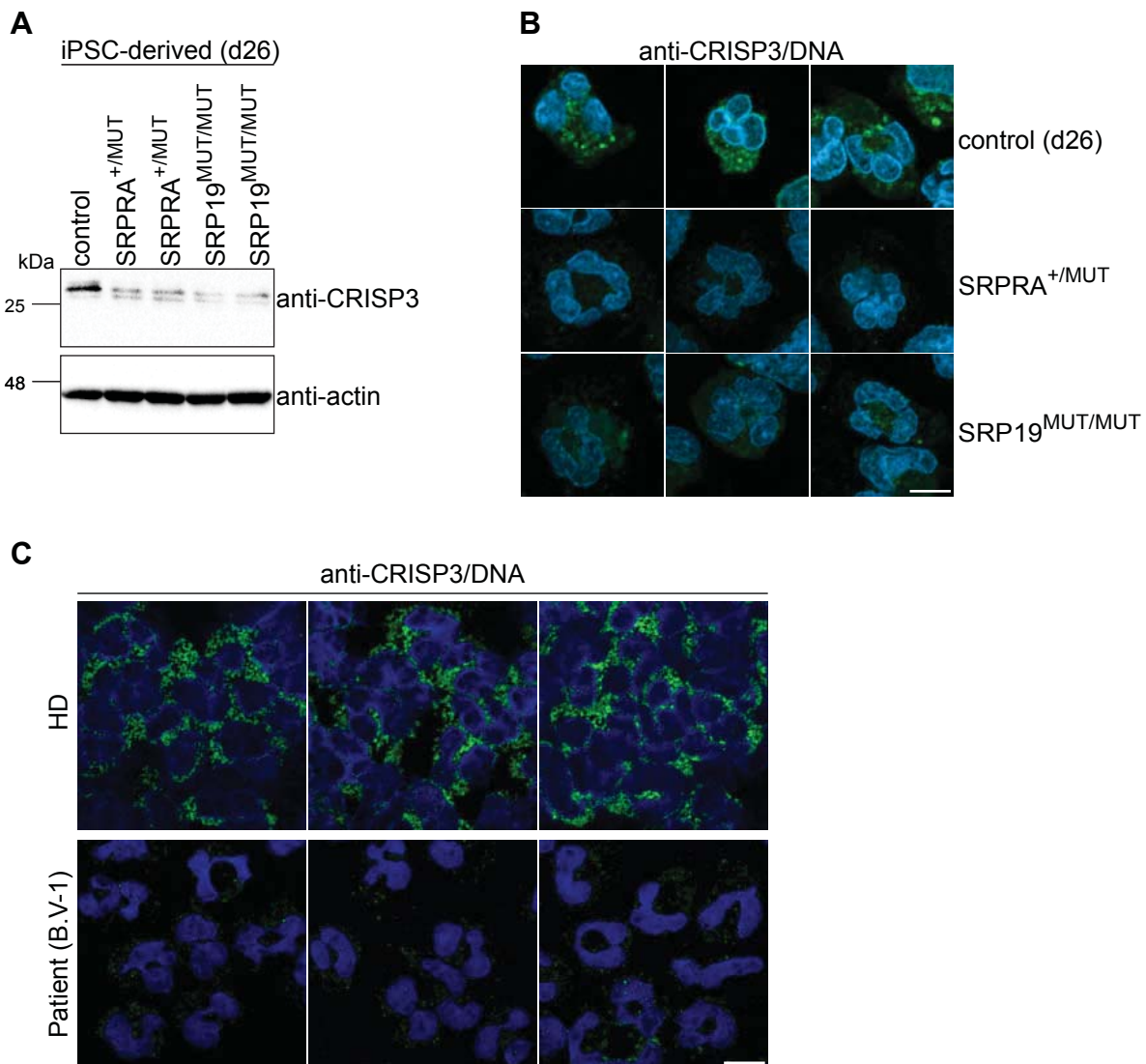
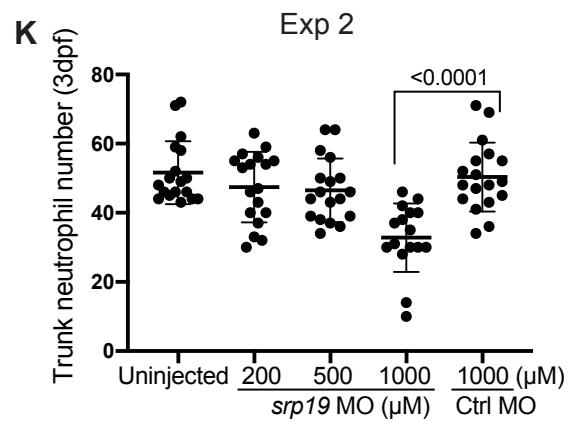
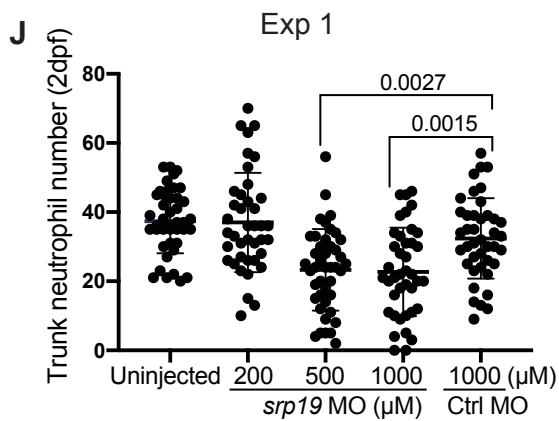
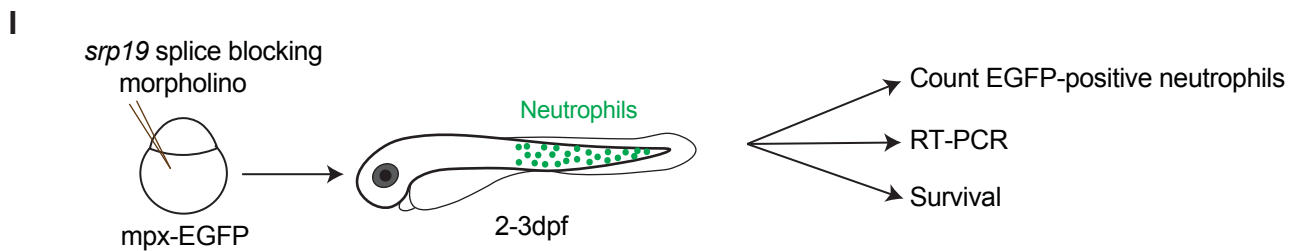
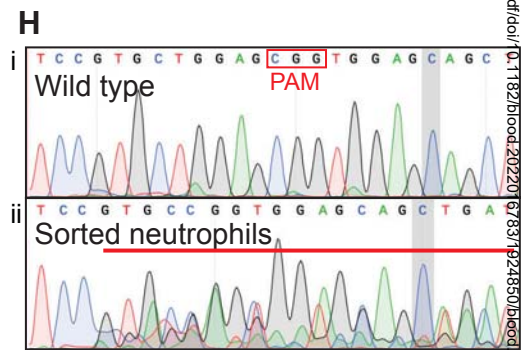
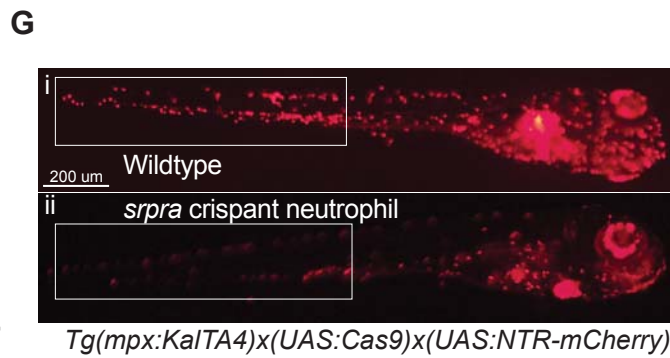
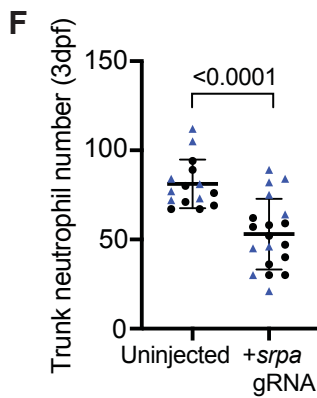
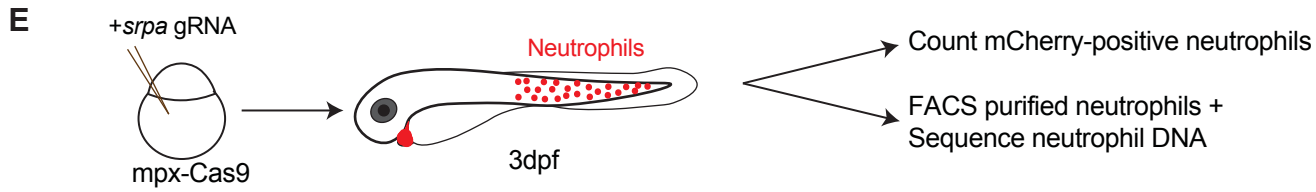
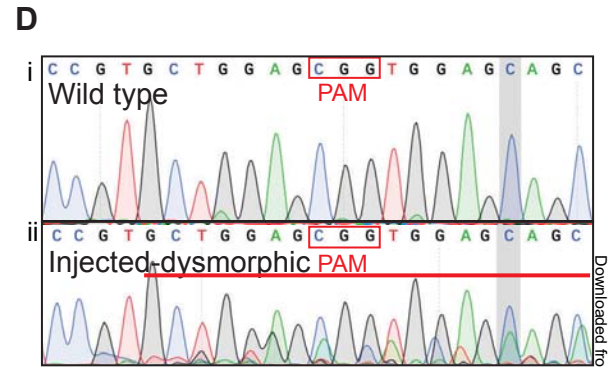
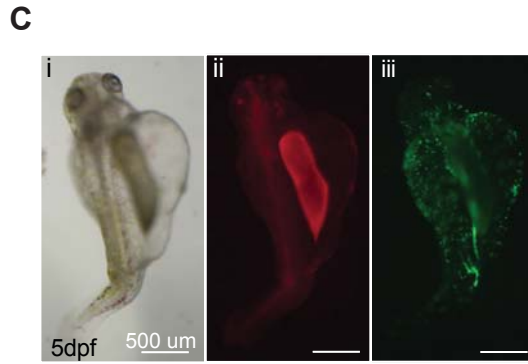
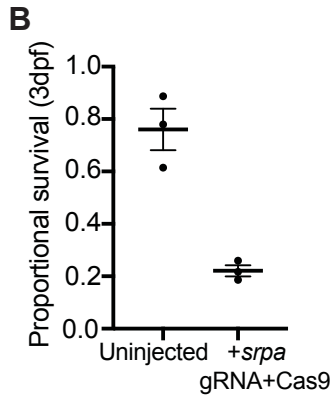
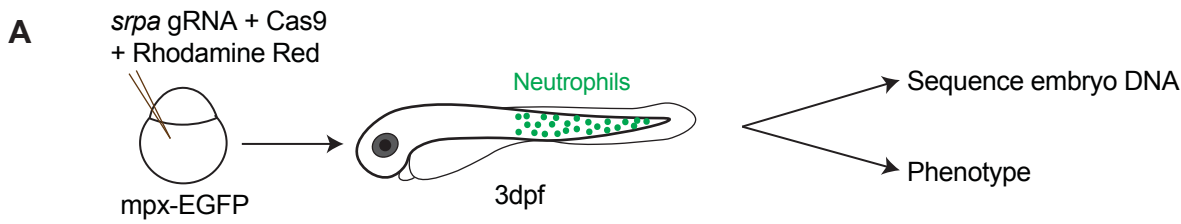
Figure 4

Figure 5





Title

Human genetic defects in SRP19 and SRPRA cause severe congenital neutropenia with distinctive proteome changes

Authors

Monika I. Linder^{1,†}, Yoko Mizoguchi^{1,10,†}, Sebastian Hesse^{1,†}, Gergely Csaba², Megumi Tatematsu¹, Marcin Łyszkiewicz^{1‡}, Natalia Zięta^{1#}, Tim Jeske^{1,5}, Maximilian Hastreiter¹, Meino Rohlf¹, Yanshan Liu^{1,3}, Piotr Grabowski⁴, Kaarin Ahomaa⁵, Daniela Maier⁶, Marko Schwestka⁷, Vahid Pazhakh^{7,8}, Abdulsalam I. Isiaku⁷, Brenda Briones Miranda⁷, Piers Blombery⁸, Megumu K. Saito⁹, Ejona Rusha¹⁰, Zahra Alizadeh¹¹, Zahra Pourpak¹¹, Masao Kobayashi¹², Nima Rezaei¹³, Ekrem Unal¹⁴, Fabian Hauck¹, Micha Drukker¹⁰, Barbara Walzog⁶, Juri Rappsilber⁴, Ralf Zimmer², Graham J. Lieschke⁷ and Christoph Klein^{1,*}

Affiliations

¹Department of Pediatrics, Dr. von Hauner Children's Hospital, University Hospital, LMU, Munich, 80337, Germany; ²Institute of Bioinformatics, Department of Informatics, LMU, Munich, 80333, Germany; ³Laboratory of Genomic and Precision Medicine, Wuxi School of Medicine, Jiangnan University, Wuxi, 214122, China; ⁴Bioanalytics, Institute of Biotechnology, Technical University of Berlin, 13355, Germany; ⁵Institute of Bioinformatics and Systems Biology, Helmholtz Center Munich, Neuherberg, 85764, Germany; ⁶Department of Cardiovascular Physiology and Pathophysiology, Biomedical Center, LMU, Planegg-Martinsried, 82152, and Walter Brendel Centre of Experimental Medicine, University Hospital, LMU, Munich, 81377, Germany; ⁷Australian Regenerative Medicine Institute, Monash

University, Clayton, VIC 3800, Australia; ⁸Department of Pathology, Peter MacCallum Cancer Centre, Melbourne, VIC 3000, Australia; ⁹Department of Clinical Application, Center for iPS cell Research and Application, Kyoto University, Kyoto, 606-8507, Japan; ¹⁰Institute of Stem Cell Research and the Induced Pluripotent Stem Cell Core Facility, Helmholtz Center Munich, Neuherberg, 85764, Germany; ¹¹Immunology, Asthma and Allergy Research Institute, Tehran University of Medical Sciences, Teheran, 14194, Iran; ¹²Department of Pediatrics, Graduate School of Biomedical Sciences, Hiroshima University, Hiroshima, 734-8551, Japan; ¹³Research Center for Immunodeficiencies, Children's Medical Center, Tehran University of Medical Sciences, Tehran, 14194, Iran; ¹⁴Department of Pediatrics, Division of Pediatric Hematology & Oncology, Erciyes University, Kayseri, 38029, Turkey.

† MIL, YM and SH contributed equally to this study.

‡ present address: Department of Pediatrics and Adolescent Medicine,
University Medical Center Ulm, Ulm, Germany

present address: Cancer Immunology and Immune Modulation, Boehringer
Ingelheim Pharma GmbH & Co. KG, Biberach an der Riss, Germany

* **Correspondence:** Christoph Klein, Department of Pediatrics, Dr. von Hauner Children's Hospital, Ludwig-Maximilians-Universität München, Lindwurmstraße 4, 803377 Munich, Germany, e-mail: Christoph.Klein@med.uni-muenchen.de, phone: +49 (0)89-4400-57701, fax: +49 (0)89-4400-57702.

Key Points

- *SRPRA* and *SRP19* are novel genes affected in congenital neutropenia and essential for granule protein processing
- Comparative proteomics in neutrophil granulocytes from patients with defects in *SRPRA*, *SRP19*, *SRP54*, *HAX1*, and *ELANE* reveal genotype-specific alterations

Abstract

The mechanisms of coordinated changes in proteome composition and their relevance for the differentiation of neutrophil granulocytes are not well studied. Here, we discover two novel human genetic defects in *SRPRA* and *SRP19*, constituents of the mammalian co-translational targeting machinery and characterize their role in neutrophil granulocyte differentiation. We systematically study the proteome of neutrophil granulocytes from patients with variants in the signal recognition particle (SRP) genes, *HAX1*, and *ELANE* and identify global as well as specific proteome aberrations. Using *in vitro* differentiation of human induced pluripotent stem cells and *in vivo* zebrafish models, we study the effects of SRP-deficiency on neutrophil granulocyte development. In a heterologous cell-based inducible protein expression system, we validate the effects conferred by SRP dysfunction for selected proteins that we identified in our proteome screen. Thus, SRP-dependent protein processing, intracellular trafficking and homeostasis are critically important for the differentiation of neutrophil granulocytes.

Introduction

Neutrophil granulocytes play sophisticated roles in the regulation of anti-microbial host defense, cancer and chronic inflammation^{1,2}. They execute their main function by the usage of proteins stored in a heterogeneous set of granules, including primary, secondary, ficolin-rich and tertiary granules³.

Granule proteins synthesis is tightly linked to the highly ordered differentiation of pluripotent hematopoietic stem cells (HSCs) into mature neutrophil granulocytes³.

Studying patients with rare genetic diseases has proven powerful to highlight novel genes and pathways orchestrating the development and function of neutrophil granulocytes^{4,5}. Severe congenital neutropenia (SCN) comprises a clinically and genetically heterogeneous spectrum of rare inherited disorders characterized by impaired maturation of neutrophil granulocytes⁴. Originally identified by Rolf Kostmann⁶, patients with autosomal recessive congenital neutropenia have mutations in the mitochondrial protein HCLS1-associated protein X-1 (HAX1)⁷. The genes encoding the ER-resident proteins Glucose-6-phosphate translocase (G6PC3) and Jagunal Homolog 1 (JAGN1) are also involved in maintaining physiological neutrophil differentiation^{8,9}. Monoallelic mutations affecting *ELANE*¹⁰ or the *Signal recognition particle 54 (SRP54)*^{11,12} are common causes of SCN and involve homeostasis of the endoplasmic reticulum (ER), as evidenced by increased ER-stress in mutated myeloid cells^{13,14}.

We here discover two novel human monogenic defects in *SRPRA* and *SRP19* affecting differentiation of neutrophil granulocytes. *SRPRA* encodes the soluble subunit of the eukaryotic SRP receptor (SR) that recognizes the SRP, a universally conserved protein machinery. The SRP is composed of seven subunits (consisting of the six polypeptides: SRP9, SRP14, SRP19, SRP54, SRP68 and SRP72, and a non-

coding RNA) and couples the synthesis of nascent proteins, which emerge from the ribosome, to the ER¹⁵. SR is a heterodimeric complex composed of a cytosolic SR α subunit (SRPRA) that interacts with the SRP and a transmembrane SR β subunit that localizes SRPRA to the ER¹⁶. The SRP subunit SRP54 (mutated in a Shwachman-Diamond-like syndrome (see Carapito et al.¹¹) and SRPRA coordinate their GTPase activity in concert to ensure the precise targeting of nascent polypeptides into the ER^{16,17}. Misfolded proteins that are unable to enter the ER are recognized and targeted for proteasomal degradation^{18,19}.

We compare the protein contents of neutrophil granulocytes from SCN patients with variants in SRPRA, SRP19, SRP54, ELANE, and HAX1 and identify genotype-specific differences as well as an essential and non-redundant role of the signal recognition particle (SRP) complex and its receptor SRPRA in human granulopoiesis.

Methods

Human subjects

We present clinical, genetic and biological data from 6 pedigrees with 11 patients carrying variants in SRP-complex subunits. A novel heterozygous *de novo* mutation in SRPRA was found in one pedigree with one patient (family A: II.3). A novel homozygous mutation in SRP19 was identified in two related pedigrees with 5 patients affected (family B: IV.2; IV.3; IV.5 and V.1; V.2). SRP54 variants were found in three pedigrees with 5 patients. A detailed description on gene variant identification is given in the supplemental methods.

Maintenance and differentiation of human iPS cells

iPS cells were maintained on a tissue culture dish coated with growth factor-reduced Matrigel (Corning, cat# 356231) in mTeSR1 serum-free medium (Stemcel, cat# 5850). Differentiation towards neutrophil-like granulocytes was initiated according to our outlined protocol in supplemental Figure 4A.

Proteome analysis

Proteome analysis was conducted as described in²⁰ (supplemental Figure 6A). Primary neutrophil granulocytes were isolated from fresh venous blood by negative selection (Miltenyi, cat# 130-104-434) and erythrocyte depletion (Miltenyi, cat# 130-098-196) yielding a final purity of > 96%. Pellets of 1×10^6 cells were frozen in 5ul of 25x protease inhibitor (Roche, cat# 04693159001) and stored in liquid nitrogen. Peptides were extracted from the pellets using Filter-Aided Sample Preparation (FASP, according to 30259475) and trypsin digestion (Thermo Fisher, cat# 90057). Using 2ug of peptides per sample, spectra were measured by a Thermo Fisher QExactive HF mass spectrometer employing a data independent acquisition approach²¹. Protein identification and quantification from raw data was based on

Biognosys Spectronaut version 14, resulting in a total of 5494 proteins, 3624 of which were reliable quantified in each sample. A detailed description is outlined in the supplemental methods.

Results

Discovery of human SRPRA and SRP19 deficiency

Our index patient (A.II-3), a five-year-old Romanian girl, suffered from failure to thrive and recurrent pulmonary infections (see supplemental Table 2 for further clinical details). She presented with growth failure, bronchiectasis (Figure 1A), pancreatic insufficiency and congenital neutropenia associated with myeloid maturation arrest in the bone marrow (supplemental Figure 1A). Electron microscopy studies of her neutrophil granulocytes showed a significant reduction of electron-dense granules (Figure 1B-C). In search of an underlying mutation, we performed whole-genome sequencing of the core family (Figure 1D). Approximately 6,000,000 genetic variants were found in the Whole-Genome-Sequencing data of seven family members. Variant filtering and prioritization revealed only two variants with combined annotation dependent depletion scores (CADD) higher than 25 (supplemental Table 1). These de novo variants were identified in *METTL26* (C16orf13, chr16: g.686265C>T, p. (Arg9Gln)) and in *SRPRA* (chr11:g.126134989G>C, p. (Gln464Glu)), respectively. Since *METTL26* is not expressed in neutrophil granulocytes²², we focused on *SRPRA* that is highly expressed in neutrophil granulocytes (Figure 3Ec). For validation, we performed Sanger sequencing for *SRPRA* in 6 family members (Figure 1D) and confirmed the mutation to be heterozygous and de-novo in the patient. Of note, the G>C point mutation in *SRPRA* results in an amino acid exchange (glutamine to glutamic acid, position 464) in an

alpha helix loop close to the GTPase active center known to mediate interaction with the cognate binding partner SRP54. Modeling the side chain substitution with PyMOL indicates that a hydrogen bond to GTP is lost, which might impair GTP hydrolysis and/or SRP complex function (Figure 1E, 1F). In search of additional SCN patients with variants in SRP-subunits (SRP9, SRP14, SRP19, SRP54, SRP68, SRP72) and in the SRP receptors (SRPRA and SRPRB) we screened our in-house database (including a total of 278 patients at the date of search) and identified 5 patients with rare heterozygous variants in *SRP54* as well as 5 patients with a homozygous splice-site variant in *SRP19* (Figure 1G and supplemental Table 1). The Human Splicing Finder predicted that the variant causes an alteration of the splice donor site with a high likelihood of causing an effect on protein splicing²³.

To provide functional proof of the significance of the SRP19 splice-site variant, we generated an artificial minigene with exons 2, 3, and 4 (supplemental Figure 1C). Upon expression in HeLa or HEK293T cells, the vector with the *SRP19* wildtype minigene gave rise to only one transcript, whereas the patient-specific *SRP19* mutation resulted in partial skipping of exon 3 (Figure 1H, supplemental Figure 1D). To confirm aberrant splicing in patients' cells, we next designed a set of primer pairs to amplify distinct SRP19 transcripts (supplemental Figure 2A) from cDNA. Whereas EBV-LCL cells from healthy individuals predominantly expressed SRP19 isoform 1, EBV-LCL cells from patients with homozygous splice site variants in *SRP19* showed reduced expression of SRP19 isoform 1 and instead additional expressed isoform 3 (supplemental Figure 2B). Similar skewing of SRP19 transcripts was observed in primary neutrophil granulocytes from SRP19-mutated patients (supplemental Figure 2C). Anti-SRP19 immunoblot studies confirmed decreased SRP19 protein expression in EBV-LCL cells from patient (B.V-1) (Figure 1I). To validate the effects of aberrant

SRP19 splicing, we generated expression vectors of GFP-SRP19 fusion constructs and transfected HeLa cells. Cells were co-stained with eIF6 (to visualize nucleoli), the ER marker Calnexin, and the DNA marker DAPI. Whereas GFP-SRP19-isoform 1 was detected in nucleoli>nuclei>cytoplasm, GFP-SRP19-isoform 3 was not found in the cytoplasm (supplemental Figure 3). These studies confirm aberrant expression of SRP19 isoforms resulting from the identified splice-site variant.

Functional validation of genomic studies

Clinical and molecular studies strongly suggested a pathogenic role for novel variants in *SRPRA* and *SRP19*. To provide functional evidence, we set up an *in vitro* differentiation system allowing us to model the genetic defects in human SRP complex subunits and its receptor SRPRA on granulopoiesis. We refined a previously published protocol²⁴ allowing us to differentiate neutrophil granulocytes *in vitro* from induced pluripotent stem cells (iPSCs). Hematopoietic cytokines (supplemental Figure 4A) induced differentiation into *neutrophil-like* neutrophil granulocytes, as indicated by FACS-based cell surface marker analysis (Figure 2A) and microscopy studies of Giemsa-stained cells (Figure 2C, left panel). In contrast to undifferentiated iPS cells, *in vitro* differentiated neutrophil granulocytes expressed myeloid cell-specific genes such as *ELANE*, *RUNX1*, *MPO*, *AZU1*, and *CSF3R* (supplemental Figure 4B). They displayed NADPH oxidase activity (supplemental Figure 4C) and showed bactericidal activity similar to neutrophil granulocytes isolated from healthy volunteers (supplemental Figure 4D). They also revealed adhesion and migration characteristics indistinguishable from peripheral blood neutrophil granulocytes isolated from healthy volunteers (supplemental Figure 4E-H). Having established this modeling system, we introduced patient-specific variants (monoallelic *SRPRA* c.1390C>G and biallelic *SRP19* c.189 +5G>A) into wildtype iPSC cells (supplemental

Figure 5B, C). As a positive control, we generated iPS cells deficient in HAX1 expression (HAX1-KO) (supplemental Figure 5D). Wildtype and mutant iPS clones that had similar expression of Oct4 and SSEA4 were chosen for *in vitro* differentiation (supplemental Figure 5E). SRPRA and SRP19 mutated iPS cells were characterized by a maturation defect of developing neutrophil granulocytes (Figure 2B), evident by an increase in myeloid progenitor cells such as promyelocytes (Figure 2C-E). A series of colony-forming unit assays with iPSC-derived CD34+/CD45+ cells confirmed a decreased ability of SRP-mutant cells to differentiate into neutrophil granulocytes (supplemental Figure 4I). Next, we examined whether the decrease in neutrophil granulocyte formation was associated with UPR activation and increased cell death. We analyzed the presence of spliced Bip and XBP1, key regulators in UPR signaling during ER stress. On day 14 of the neutrophil granulocyte differentiation protocol, SRP-mutant cells displayed activated UPR, as shown by an increased BiP protein expression in SRP-mutated cells (supplemental Figure 4J) and a significant enrichment of the spliced (s) form of XBP-1 (Figure 2F and supplemental Figure 5A). Activated UPR was concomitant with an increase in Annexin-V positive cells in SRP-mutated iPS cells (Figure 2G). Moreover, we observed an increase in cleaved PARP and cleaved caspase-3 in SRP-mutated progenitor cells (Figure 2H) suggesting that a defect in SRP19 and SRPRA leads to increased susceptibility to apoptosis.

Proteome signatures of primary neutrophil granulocytes from patients with variants in SCN genes

Adapting our previously described pipeline²⁰, we performed data-independent acquisition²¹ mass-spectrometry based deep proteome profiling of primary neutrophil granulocytes (supplemental Figure 6A). We analyzed primary neutrophil proteomes from patients with variants in SRPRA (n=1 with 3 biological replicates [1a, 1b, 1c]

sampled weeks apart), SRP19 (n=5) and SRP54 (n=4) as well as ELANE (n=5), HAX1 (n=3) together with a healthy donor cohort of 48 individuals. Principal component analysis of PC1 and PC2 (Figure 3A) separates proteomes from SCN patients and healthy individuals. We performed k-means cluster analysis to test grouping of patient samples (Figure 3B). While k1 contains all proteomes from patients with mutations in *ELANE* and *HAX1*, k2 contains exclusively proteomes from patients with mutations in *SRPRA*, *SRP54* and *SRP19*. For validation, we performed coefficient controlled agglomerative hierarchical clustering (AGNES, Figure 3C), resulting in a first cluster with all ELANE and HAX1 samples and a second cluster containing exclusively the SRP patient samples. We conclude that mutations in different subunits of the SRP result in largely overlapping proteome changes in human neutrophils that are clearly distinguishable from proteome aberrations caused by mutations in *ELANE* or *HAX1*.

To further quantify proteome aberrations, we performed differential expression analysis comparing patient-specific genotypes to healthy donors (Figure 3D a-e) as well as the ELANE/HAX1 (SCN) cluster and the SRP cluster (Figure 3D f). SRPRA and SRP54 show the largest fraction of differentially expressed proteins. SRPRA mutated neutrophil granulocytes had 631 proteins showing decreased abundance and 549 proteins showing increased abundance. Neutrophil granulocytes with mutations in *SRP54* (down 673 / up 570) and SRP19 (down 410 / up 408) also revealed markedly disturbed proteome profiles. By contrast, the changes in protein expression in HAX1-deficient neutrophils (down 384 / up 375) and ELANE-mutated neutrophils (down 352 / up 305) appeared less prominent.

Proteins showing less abundant expression in SRP genotypes were CRISP3, PTX3, LILRB1, CAMP and MMP9. Next, we analyzed the expression levels of the

respective gene products in our proteome dataset. Only SRP19 mutant neutrophil granulocytes showed a reduced protein abundance of SRP19, SRP54, and SRP68, whereas all other genotypes (SRPRA, SRP54, ELANE and HAX1) showed increased abundance of SRP proteins (Figure 3E). Neutrophil elastase protein levels were reduced in all genotypes (Figure 3Ef).

GO-term enrichment analysis revealed that regardless of the specific phenotype, numerous subcellular compartments, pathways and cellular functions are affected (Figure 3F,G). Whereas granule proteins showed reduced expression levels (Figure 3I), mitochondria, the translational apparatus, ROBO receptor signaling, ER-stress and nonsense mediated decay showed increased expression levels (Figure 3H). No genotype-specific GO-term signature could be identified.

Next, we annotated every protein to its specific location by unifying information from uniprot, gene-ontology (GO) and the human protein atlas in addition to previously published results on the proteome of specific neutrophil compartments^{25,26} and made use of a proteome ruler approach²⁷ to derive the total protein number and mass for each cellular compartment in patient and healthy donor neutrophils (Figure 3J - K).

This cellular compartment-specific view confirmed that protein expression level differences between neutrophils from patients are most striking in the granule compartment, whereas differences in other subcellular compartments were less pronounced (Figure 3J). Specifically, SRP genotypes were characterized by a marked reduction of primary granule proteins when compared to HAX1 and ELANE mutated neutrophil granulocytes. (Figure 3K)

Since SRP-deficient yeast cells are characterized by reduced expression of proteins with strongly hydrophobic N-terminals²⁸, we analyzed the N-terminal hydrophobicity scores of the underexpressed proteins in all genotypes (Figure 3L, supplemental

Figure 6 B-C). In contrast to yeast, we could not document a specific underrepresentation of proteins with hydrophobic N-terminal domains in neutrophil proteomes from patients with SRP mutations.

Functional validation of proteomic studies

To provide functional proof that decreased expression of proteins in SRP/SRPRA-mutant neutrophil granulocytes is indeed a consequence of aberrant posttranscriptional protein dynamics, we generated a series of tet-responsive HeLa cell lines allowing us to control expression kinetics of newly synthesized GFP fusion proteins (HeLa-Flp-In/T-Rex)²⁹ (supplemental Figure 7A). Upon tetracycline induction, reporters were expressed in their mature forms as indicated by the glycosylated form of CRISP3 (supplemental Figure 7A marked with an asterisk). We treated reporter cells with siRNAs directed against SRPRA, SRP19 and SRP54 (supplemental Figure 7B-D) and subsequently induced expression of transgenic reporter constructs to monitor the effect of SRP depletion on the maturation of newly synthesized secretory proteins (Figure 4A-D). Preprolactin, a secretory protein containing a prototypical signal sequence, served as control. In accordance with previous studies^{18,30}, prolactin was expressed in its mature form in control cells (Figure 4A, supplemental Figure 7A) but was not appropriately processed in cells depleted for SRPRA, SRP19 and SRP54, respectively (Figure 4A). Similarly, expression of newly synthesized GUSB-GFP and PTX3-GFP expression was markedly reduced upon knockdown of SRP components (Figure 4B-C). We also studied CRISP3, a cysteine-rich secretory glycoprotein stored in secondary granules^{31,32}. As shown in Figure 4D, CRISP3, expressed with reduced abundance in primary neutrophil granulocytes from SRP-deficient patients (see Figure 3B-C), was also decreased upon knockdown of SRPRA, SRP19 or SRP54 in HeLa cells. The

expression of the nuclear pore complex (NPC) constituent GFP-Nup53 was not affected upon SRP depletion (supplemental Figure 7E). Finally, we studied the SRP-dependency of intracellular trafficking of PTX3 and CRISP3 fusion proteins. The PTX3-GFP fusion protein was enriched throughout the entire ER with partial co-localization with Calnexin in control cells (Figure 4E) while it was markedly reduced upon knockdown of SRPRA, SRP19 or SRP54. In control cells CRISP3-GFP accumulated in close proximity to the Golgi, as evidenced by co-localization with the cis-Golgi matrix protein GM130³³, however, siRNA-mediated depletion of SRPRA, SRP19 and SRP54 prevented proper trafficking (Figure 4F-G). Thus, these data indicate that the SRP is essential for targeting, processing and distribution of the granule proteins PTX3 and CRISP3.

Next, we examined the expression and localization of CRISP3 in neutrophil granulocytes (day26) derived from control, SRPRA^{+MUT} and SRP19^{MUT/MUT} iPS cells. SRPRA^{+MUT} and SRP19^{MUT/MUT} neutrophils cells showed a decrease of endogenous CRISP3 expression (Figure 5A-B). Of note, the mature, glycosylated form of CRISP3 was reduced in SRPRA^{+MUT} and SRP19^{MUT/MUT} neutrophil-like granulocytes while concurrently the unglycosylated form of CRISP3 was more abundantly expressed (Figure 5A). Notably, a reduction of CRISP3 expression was also observed by immunofluorescence in primary neutrophil granulocytes from the SRP19 patient (B.V-1) compared to a healthy donor (Figure 5C).

Zebrafish models of SRPRA and SRP19 deficiency

To confirm our observations in an *in vivo* model, we targeted the zebrafish SRPRA ortholog *srpra* in zebrafish embryos by a CRISPR/Cas9 gene editing approach designed to disrupt *srpra* (supplemental Figure 8A).

F0 crispant embryos displayed severe developmental deformities and high embryonic lethality (Figure 6A-C), which precluded quantitative evaluation of neutrophil abundance. On-target *srpra* gene editing in these embryos was verified by Sanger sequencing, which demonstrated a complex pattern of assorted gene-edited alleles around the targeted PAM site, confirming that the gene editing approach was efficacious as designed (Figure 6D). To circumvent these general developmental effects of global *srpra* gene disruption *in vivo*, we selectively knocked down *srpra* in neutrophils using our neutrophil-specific gene editing line *Tg(mpx:KalTA4) x (UAS:Cas9) x (UAS:NTR-mCherry)*, in which Cas9 expression is confined to mCherry-marked neutrophils by a myeloperoxidase promoter-driven compound transgenic system³⁶ (Figure 6E). *Srpra*-gRNA delivery to these embryos significantly reduced neutrophil abundance at 3 dpf by 35% (Figure 6F-G). The mCherry-positive neutrophils remaining in these embryos were purified by FACS for Sanger sequencing (Figure 6H, supplemental Figure 8B), which confirmed on-target gene editing in these residual neutrophils. NGS demonstrated the commonest variant to be an 8 nt deletion (VAF=13%) resulting in a frameshift mutation (supplemental Figure 8C). Although the gene editing strategy employed provided opportunity for generating a zebrafish equivalent of the candidate missense disease allele by homology-directed repair following CRISPR/Cas9 editing (supplemental Figure 8A), this did not occur at a detectable frequency in the F0 crispants.

To mimic the biallelic exon 3 splice site mutation of SRP19 found in patients, the exon 3 splice donor site of zebrafish *srp19* was targeted by a splice-blocking morpholino (MO) for global disruption of *srp19* splicing (Figure 6I, supplemental Figure 9A). On-target *srp19*-MO action was confirmed by RT-PCR, which demonstrated reduced levels of the PCR product corresponding to the normal

transcript at all MO doses (supplemental Figure 9B-C), and also a MO-dose-dependent increase in an aberrant PCR product corresponding to intron 3 retention, which was confirmed by Sanger sequencing (supplemental Figure 9D). At the highest MO dose injected, *srp19*-MO-injected embryos demonstrated mild developmental defects not seen with control MO (absent swim bladder, curved tails and reduced 2 dpf survival; supplemental Figure 9E-F), but were scorable for neutrophil numbers at all MO doses. *srp19*-MO-injected embryos had significantly reduced neutrophil numbers in a MO-dose-dependent fashion, both at 2 dpf for injectate concentrations of 500 μ M (where development and survival were normal) and at 2 and 3 dpf for 1000 μ M (where development was perturbed and survival was reduced) (Figure 6J-K).

Collectively, these two animal models of transient loss-of-function support the hypothesis that normal levels of *srpra* and *srp19* function are required for normal granulopoiesis *in vivo*, and add to the genetic evidence that the SRPA and SRP19 mutations in these patients are responsible for their neutropenia.

Discussion

In this study we describe two novel human genetic defects in SRP19 and SRPRA, components of the co-translational targeting machinery. Clinically, both SRP19- and SRPRA-deficiencies are characterized by severe congenital neutropenia associated with a myeloid maturation arrest resembling the neutrophil phenotype of SRP54-deficiency^{11,12}.

During the initial steps of SRP biogenesis, SRP19 interacts with specific sites on the SRP RNA in the nucleolus and promotes the association of other SRP components. The assembly of this nuclear export-competent pre-SRP is prerequisite for the binding of SRP54 to helix 8 of the SRP RNA in the cytoplasm (reviewed in³⁴). Consistent

with a previous study³⁵ we observed GFP-SRP19 not only in the cytoplasm where the mature SRP resides, but also in the nucleoplasm and the nucleolus whereas the identified splice-site variant in SRP19 abolished the cytoplasmic localization of the expressed isoform. Moreover, the expression of SRP19 was reduced in patients' cells. It could be hypothesized that the identified splice-site variant causes a reduction of SRP19 and hence impacts on stable formation of the pre-SRP complex or its export into the cytoplasm, as also seen in studies of yeast SRP biogenesis that critically depend on adequate endogenous levels of Sec65p (SRP19 homolog of yeast). Levels of endogenous SRP19 might be also critical for robust core-SRP assembly by guiding the efficient binding of SRP54 and its stable association with the SRP.

To study the effects of the SRPRA and SRP19 variants on granulopoiesis, we engineered iPS cells using CRISPR/Cas9 gene editing and thus modeled the mono-allelic SRPRA variant (Q464E) as well as the bi-allelic splice-site variants in SRP19. iPS cells with variants in either SRPRA, SRP19 or deficient in HAX1 expression had a significantly reduced capacity to differentiate into neutrophil granulocytes compared to WT iPS cells, providing evidence that both SRPRA and SRP19 are required for granulopoiesis. Recently, a comprehensive gene editing strategy in human hematopoietic stem and progenitor (HSP) cells associated ELANE mutations with their efficiency to restore neutrophil maturation and HSPC function³⁶.

The neutrophil differentiation process is tightly linked to the regulation of granule protein synthesis³. Mass-spectrometry based deep-proteome analysis allows the characterization of cellular protein composition in high detail, including neutrophil granulocytes^{26,37}. Rieckmann et al.²² have recently published, among other leucocytes, an ultra-deep analysis of peripheral blood neutrophil granulocytes. They quantified 6007 proteins in 3 samples while our study quantified 3624 proteins with at least 2

peptides in each of our 68 samples. The overlapping data show a Pearson correlation coefficient (PCC) of 0.7, indicating strong correlation between their data and ours (data not shown). We have previously shown that proteome profiles of neutrophil granulocytes promise to help to unravel the effects and specificities of monogenic defects. Here, we provide the first comprehensive proteomic analysis of neutrophil granulocytes from patients with variants in SRP/SRPRA, ELANE, and HAX1.

Independent of the genetic variant, all neutrophil granulocytes were characterized by strong imbalances of their proteome. Whereas proteins of the translational apparatus, mitochondrial proteins and stress response proteins (ER stress and nonsense-mediated decay) were more abundantly expressed in patient derived neutrophils, proteins from all granule subsets were less abundantly expressed. These global changes may reflect incomplete terminal differentiation and/or cellular adaption to the consequences of the underlying mutation (e.g. unfolded protein response to variants in neutrophil elastase, see Grenda³⁸). Even though no pathognomonic proteome aberrations could be established, our proteome analysis revealed pronounced loss of proteins of neutrophil granules, including CRISP3 and PTX3. Proper SRP function might emerge as a rate-limiting step to secure timely and efficient production of defined granule proteins, a prerequisite for physiological neutrophil maturation.

A requirement for intact SRP function to sustain normal granulopoiesis in larval zebrafish *in vivo* has been established in studies examining the global genetic requirement of *srp54* in zebrafish development^{11,14} and modelling specific *SRP54* disease alleles¹⁴. We therefore used zebrafish granulopoiesis as a bioassay to evaluate the requirement for *srpra* and *srp19* in neutrophil production. Crispants of the *srpra* locus (with assorted disruptive gene edits) phenocopied the embryonic lethality of the zebrafish *srp54* knockout⁴⁶. To circumvent this, we gene-edited *srpra* in a neutrophil-

lineage restricted manner using our system that limits Cas9 expression to maturing neutrophils using the *myeloperoxidase* promoter³⁹. The neutrophil deficiency of these lineage-specific crispants demonstrated a requirement for normal *srpra* function in granulopoiesis *in vivo*. Similarly, *srp19* morphants with confirmed intron 3 retention (predicted to result in a nonsense transcript) confirmed a requirement for normal *srp19* splicing in sustaining normal granulopoiesis *in vivo*. Although these strategies did not replicate the exact disease allele variants, these data represent a formal reverse genetic test of gene requirement *in vivo*, and functionally support the candidacy of *SRPRA* and *SRP19* as SCN disease genes. Collectively, these observations are consistent with mutation of *SRP54* and several other *SRP* components being causative of an SCN disease phenotype.

Acknowledgments

We thank all patients and their families for allowing us to study their cells and all clinical staff taking excellent care. We are particularly indebted to Dr. Sorin Iurian (Romania) for referring family A and dedicate this work in memory of our patient A-II-3 who tragically died in December 2021. We acknowledge Sebastian Hollizeck and Isabelle Plonner for outstanding expertise in the C4R sequencing and computational facility. We are very grateful to Prof. Thomas U. Mayer for providing the HeLa-Flp-In/T-Rex cell line. We thank Mrs. Tanja Vlaovic for isolating neutrophils from healthy volunteers. We thank Dr. Diana Laverde for her guidance in performing the phagocytosis assay. We acknowledge Prof. Manfred Rohde (Helmholtz Centre for Infection Research, Department of Medical Microbiology, Braunschweig, Germany) for the acquisition and processing of electron microscopy studies. We are very grateful to the Pediatric Radiology team at LMU for acquisition of the CT scan. We thank Drs Lucy Fox and Ella Thompson for help with the zebrafish NGS analysis.

This work was supported by grants from the DFG (Gottfried Wilhelm Leibniz Program, CRC914 project A08 and A02), the BMBF (PIDNET) and the Care-for-Rare Foundation. The Sir Peter MacCallum Cancer Centre Molecular Hematology Laboratory is supported by funding from Wilson Centre for Lymphoma Genomics through the Snowdome Foundation. The Australian Regenerative Medicine Institute is supported by grants from the State Government of Victoria and the Australian Government. Graham Lieschke was supported by the National Health and Medical Research Council (1044754, 1086020, 1159278) and Graham Lieschke, Christoph Klein and Piers Blombery were supported by Maddie Riewoldt's Vision (ARMI-MRV-2018G). Members of the Lieschke Lab are supported by grants of the Monash University (Graduate Scholarship and International Tuition Scholarship).

Whole-genome sequencing on family A was supported by the Junior Researcher Fund of LMU Excellence Initiative (to N.Z.).

Authorship

Contribution: Original idea: C.K.; Conceptualization and Methodology: C.K. M.I.L. Y.M., S.H., R.Z.; Clinical and patient-related investigations: C.K., S.H., A.Z., M.K., N.R., E.Ü., F.H.; Experimentation: M.I.L., Y.M., S.H., M.T., N.Z., M.R., Y.L., P.G., D.M., M.S., E.R., M.D.; M.S.; A.I.I., B.B.M.; Computational analysis: S.H., G.C., A.K., T.J., M.H., R.Z.; Resources: M.D., B.W., J.R., R.Z., C.K.; P.B., G.J.L.; Data Curation: C.G., R.M. R.Z.; M.S.; Writing Original Drafts: C.K., M.I.L., S.H., Y.M.; G.J.L.; Supervision: C.K., B.W., V.P., R.Z., J.R.; G.J.L.; Writing, Review & Editing of draft, all authors; All authors read and approved the manuscript before submission.

Conflict-of-interest disclosure

The authors declare no competing financial interests.

Correspondence

Christoph Klein, Department of Pediatrics, Dr. von Hauner Children's Hospital, University Hospital, LMU, Munich, 80337, Germany; e-mail: christoph.klein@med.uni-muenchen.de.

References

1. Mantovani A, Cassatella MA, Costantini C, Jaillon S. Neutrophils in the activation and regulation of innate and adaptive immunity. *Nat Rev Immunol*. 2011;11(8):519-531.
2. Nauseef WM, Borregaard N. Neutrophils at work. *Nat Immunol*. 2014;15(7):602-611.
3. Cowland JB, Borregaard N. Granulopoiesis and granules of human neutrophils. *Immunol Rev*. 2016;273(1):11-28.
4. Klein C. Genetic defects in severe congenital neutropenia: emerging insights into life and death of human neutrophil granulocytes. *Annu Rev Immunol*. 2011;29:399-413.
5. Klein C, Gahl WA. Patients with rare diseases: from therapeutic orphans to pioneers of personalized treatments. *EMBO Mol Med*. 2018;10(1):1-3.
6. Kostmann R. Infantile genetic agranulocytosis; agranulocytosis infantilis hereditaria. *Acta Paediatr Suppl*. 1956;45(Suppl 105):1-78.
7. Klein C, Grudzien M, Appaswamy G, et al. HAX1 deficiency causes autosomal recessive severe congenital neutropenia (Kostmann disease). *Nat Genet*. 2007;39(1):86-92.
8. Boztug K, Appaswamy G, Ashikov A, et al. A syndrome with congenital neutropenia and mutations in G6PC3. *N Engl J Med*. 2009;360(1):32-43.
9. Boztug K, Jarvinen PM, Salzer E, et al. JAGN1 deficiency causes aberrant myeloid cell homeostasis and congenital neutropenia. *Nat Genet*. 2014;46(9):1021-1027.
10. Dale DC, Person RE, Bolyard AA, et al. Mutations in the gene encoding neutrophil elastase in congenital and cyclic neutropenia. *Blood*. 2000;96(7):2317-2322.
11. Carapito R, Konantz M, Paillard C, et al. Mutations in signal recognition particle SRP54 cause syndromic neutropenia with Shwachman-Diamond-like features. *J Clin Invest*. 2017;127(11):4090-4103.

12. Bellanne-Chantelot C, Schmaltz-Panneau B, Marty C, et al. Mutations in the SRP54 gene cause severe congenital neutropenia as well as Shwachman-Diamond-like syndrome. *Blood*. 2018;132(12):1318-1331.
13. Nanua S, Murakami M, Xia J, et al. Activation of the unfolded protein response is associated with impaired granulopoiesis in transgenic mice expressing mutant Elane. *Blood*. 2011;117(13):3539-3547.
14. Schürch C, Schaefer T, Müller JS, et al. SRP54 mutations induce congenital neutropenia via dominant-negative effects on XBP1 splicing. *Blood*. 2021;137(10):1340-1352.
15. Akopian D, Shen K, Zhang X, Shan SO. Signal recognition particle: an essential protein-targeting machine. *Annu Rev Biochem*. 2013;82:693-721.
16. Shan SO, Schmid SL, Zhang X. Signal recognition particle (SRP) and SRP receptor: a new paradigm for multistate regulatory GTPases. *Biochemistry*. 2009;48(29):6696-6704.
17. Zhang X, Shan SO. Fidelity of cotranslational protein targeting by the signal recognition particle. *Annu Rev Biophys*. 2014;43:381-408.
18. Karamyshev AL, Patrick AE, Karamysheva ZN, et al. Inefficient SRP interaction with a nascent chain triggers a mRNA quality control pathway. *Cell*. 2014;156(1-2):146-157.
19. Oh E, Akopian D, Rape M. Principles of Ubiquitin-Dependent Signaling. *Annu Rev Cell Dev Biol*. 2018;34:137-162.
20. Grabowski P, Hesse S, Hollizeck S, et al. Proteome Analysis of Human Neutrophil Granulocytes From Patients With Monogenic Disease Using Data-independent Acquisition. *Mol Cell Proteomics*. 2019;18(4):760-772.
21. Vizcaino JA, Csordas A, del-Toro N, et al. 2016 update of the PRIDE database and its related tools. *Nucleic Acids Res*. 2016;44(D1):D447-456.

22. Rieckmann JC, Geiger R, Hornburg D, et al. Social network architecture of human immune cells unveiled by quantitative proteomics. *Nat Immunol.* 2017;18(5):583-593.
23. Desmet FO, Hamroun D, Lalande M, Collod-Bérout G, Claustres M, Bérout C. Human Splicing Finder: an online bioinformatics tool to predict splicing signals. *Nucleic Acids Res.* 2009;37(9):e67.
24. Niwa A, Heike T, Umeda K, et al. A novel serum-free monolayer culture for orderly hematopoietic differentiation of human pluripotent cells via mesodermal progenitors. *PLoS One.* 2011;6(7):e22261.
25. Lominadze G, Powell DW, Luerman GC, Link AJ, Ward RA, McLeish KR. Proteomic analysis of human neutrophil granules. *Mol Cell Proteomics.* 2005;4(10):1503-1521.
26. Rørvig S, Østergaard O, Heegaard NH, Borregaard N. Proteome profiling of human neutrophil granule subsets, secretory vesicles, and cell membrane: correlation with transcriptome profiling of neutrophil precursors. *J Leukoc Biol.* 2013;94(4):711-721.
27. Wiśniewski JR, Hein MY, Cox J, Mann M. A "proteomic ruler" for protein copy number and concentration estimation without spike-in standards. *Mol Cell Proteomics.* 2014;13(12):3497-3506.
28. Hatsuzawa K, Tagaya M, Mizushima S. The hydrophobic region of signal peptides is a determinant for SRP recognition and protein translocation across the ER membrane. *J Biochem.* 1997;121(2):270-277.
29. Hafner J, Mayr MI, Mockel MM, Mayer TU. Pre-anaphase chromosome oscillations are regulated by the antagonistic activities of Cdk1 and PP1 on Kif18A. *Nat Commun.* 2014;5:4397.
30. Lakkaraju AK, Mary C, Scherrer A, Johnson AE, Strub K. SRP keeps polypeptides translocation-competent by slowing translation to match limiting ER-targeting sites. *Cell.* 2008;133(3):440-451.

31. Kjeldsen L, Cowland JB, Johnsen AH, Borregaard N. SGP28, a novel matrix glycoprotein in specific granules of human neutrophils with similarity to a human testis-specific gene product and a rodent sperm-coating glycoprotein. *FEBS Lett.* 1996;380(3):246-250.
32. Udby L, Calafat J, Sorensen OE, Borregaard N, Kjeldsen L. Identification of human cysteine-rich secretory protein 3 (CRISP-3) as a matrix protein in a subset of peroxidase-negative granules of neutrophils and in the granules of eosinophils. *J Leukoc Biol.* 2002;72(3):462-469.
33. Nakamura N, Rabouille C, Watson R, et al. Characterization of a cis-Golgi matrix protein, GM130. *J Cell Biol.* 1995;131(6 Pt 2):1715-1726.
34. Luirink J, Sinning I. SRP-mediated protein targeting: structure and function revisited. *Biochim Biophys Acta.* 2004;1694(1-3):17-35.
35. Dean KA, von Ahsen O, Görlich D, Fried HM. Signal recognition particle protein 19 is imported into the nucleus by importin 8 (RanBP8) and transportin. *J Cell Sci.* 2001;114(Pt 19):3479-3485.
36. Rao S, Yao Y, Soares de Brito J, et al. Dissecting ELANE neutropenia pathogenicity by human HSC gene editing. *Cell Stem Cell.* 2021;28(5):833-845 e835.
37. Tomazella GG, da Silva I, Laure HJ, et al. Proteomic analysis of total cellular proteins of human neutrophils. *Proteome Sci.* 2009;7:32.
38. Grenda DS, Murakami M, Ghatak J, et al. Mutations of the ELA2 gene found in patients with severe congenital neutropenia induce the unfolded protein response and cellular apoptosis. *Blood.* 2007;110(13):4179-4187.
39. Isiaku AI, Zhang Z, Pazhakh V, et al. Transient, flexible gene editing in zebrafish neutrophils and macrophages for determination of cell-autonomous functions. *Dis Model Mech.* 2021;14(7).

Figure Legends

Figure 1. Identification of SRPRA and SRP19 novel gene variants.

- (A) Chest CT Scan of index patient II-3 (family A).
- (B) Trans-electron microscopy (TEM) sections of neutrophils from index patient A.II-3 in comparison to unaffected family members (brother A.II-2, father A.I-2) and healthy donors.
- (C) Quantification of neutrophil granule content from healthy donor, A.I-2, A.II-2 and A.II-3. Group differences with $p < 0.0001$. Single group differences via student t-test. * = $p < 0.01$ / ** = $p < 0.001$ / **** = $p < 0.00001$.
- (D) Pedigree of family A and Sanger sequencing chromatograms of wildtype (WT) and the SRPRA mutation site.
- (E and F) Ribbon representation of the three-dimensional structure of the human SRPRA WT (E) and mutated SRPRA (Q464E) (F).
- (G) Pedigree of family B and Sanger sequencing chromatograms of the WT and the SRP19 mutation site.
- (H) RT-PCR results documenting WT and mutated (mut) SRP19₂₋₄ minigene transcripts in HeLa cells. F1-R1 and F1-R2 are the primer pairs used to amplify the indicated SRP19 exons. The primer pair F1-R2 amplifies SRP19 exon 2-4 as indicated with a red arrow (281 bp). The SRP19 variant results in a PCR product of only 209bp (blue arrow). The primer pair F1-R1 amplifies parts of the SRP19 Exon 2 and is used as a transfection efficiency control.

- (I) Immunoblot analysis of EBV-LCL lysates from healthy donor (HD), patient (B.V-1) and a heterozygous family member (B.IV-6). Experiment performed in triplicate.

Figure 2. Characterization of iPSC-derived neutrophil granulocytes.

- (A) Flow cytometric analysis of control iPSC-derived neutrophil granulocytes at day 29. Experiment performed in triplicate.
- (B) Quantification of live floating cells per 6 iPS colonies (per well), determined at indicated timepoints during differentiation. For control, SRPRA^{+MUT} and SRP19^{MUT/MUT} two biological replicates (2 different clones) are presented as mean of 3 independent experiments. For HAX1-knock-out (KO) the mean of one clone of 3 independent experiments is presented. Statistical analysis using 2-way ANOVA followed by Dunnett's multiple comparisons test. ** = $p < 0.0032$ / **** = $p < 0.0001$.
- (C) Light microscopy of control, SRPRA^{+MUT}, SRP19^{MUT/MUT} and HAX1-KO iPSC-derived myeloid cells stained with May-Grünwald Giemsa at day 29.
- (D) Quantification of the distribution of precursor populations in iPSC-derived myeloid cells for the indicated genotypes. Floating cells were harvested and stained with May-Grünwald Giemsa at day 29 and classified by light microscopy. The quantification was performed for two independent experiments; in sum 200 cells per genotype were classified.
- (E) Statistical analysis of the quantification shown in Figure 2D using 2-way ANOVA followed by Dunnett's multiple comparisons test. * = $p < 0.03$ / *** = $p < 0.0009$ / **** = $p < 0.0001$. Errorbars represent mean with SD. Quantification of two independent experiments are shown.

- (F) Immunoblot analysis of XBP-1s (spliced form of XBP-1) expression in iPSC-derived myeloid cells at day14. Experiment performed in triplicate.
- (G) Quantification of Annexin V positive cells in sorted (CD33high/CD49dhigh) immature iPSC-derived neutrophil granulocytes. Cells were analyzed on day 26 after differentiation. (n=3 wells per each clone, multiple t-test). For control, SRPRA^{+MUT} and SRP19^{MUT/MUT} two biological replicates (2 different clones) are presented as mean of 3 independent experiments.
- (H) Immunoblot analysis of apoptosis-specific markers (cleaved PARP and cleaved caspase3) in iPSC-derived myeloid cells at day14. Experiment performed in triplicate.

Figure 3. Proteome analysis of patient derived primary neutrophil granulocytes.

- (A) Principal component analysis showing PC1 and PC2 of neutrophil granulocyte proteomes. Each dot represents a sample and each colour represents a genotype.
- (B) Principal component analysis showing PC1 and PC2 of neutrophil granulocyte proteomes with k-means cluster results. Each dot represents a sample, each colour represents the cluster assignment to k1 or k2. Genotypes are shown as labels.
- (C) Hierarchical dendrogram showing ward-based agglomerative coefficient clustering (AGNES) of neutropenia samples with k=2. Each tree leaf represents a single sample with the two clusters framed in red and green.
- (Da-f) Volcano plots showing differentially expressed proteins of the comparisons SCN genotypes vs healthy donor (a-e) and (f) SRP vs SCN (= ELANE/HAX1). Each dot represents a protein and is located in the plot

according to its fold change (x-axis) and inverted p-value (y-axis). Dot color intensity represents increasing fold change levels. The total amount of significantly over and under expressed proteins ($\text{adj.p} < 0.05$ and $\text{abs}(\text{fold change}) > 0.5$) is written in numbers above the axis. The most extreme proteins (max 12, dependent on $\text{max} > \text{Fc}$ rank) of each genotype are labelled.

- (Ea-f)** Expression boxplots of significantly differentially expressed single SRP-complex constituents (a-e) and ELANE (f) in SCN genotypes and healthy donor (x-axis). Differential expression was first evaluated using ANOVA (a [SRP19] $p = 2.8\text{e-}9$, b [SRP54] $p = 4.9\text{e-}6$, c [SRPRA] $p = 6.3\text{e-}8$, d [SRPRB] $p = 2.2\text{e-}16$, e [SRP68] $p = 2.4\text{e-}7$, f [ELANE] $p = 2.2\text{e-}16$) and post-t-test using healthy donors as control (p value indicated with asterix, * < 0.05 , ** < 0.01 , *** < 0.001 or ns = not significant).
- (F-I)** Enrichment plots showing significant terms of each group subdivided into function groups. F: over-expressed in genotype vs healthy, G: under-expressed in genotype vs healthy, H: over-expressed in SRP vs common SCN (ELANE, HAX1) compared with SRP vs healthy, I: under-expressed in SRP vs common SCN (ELANE, HAX1) compared with SRP vs healthy. Significance threshold for protein inclusion is $\text{adj. P} < 0.05$ and $\text{abs}(\text{Fc}) > 0.5$, threshold of significant term enrichment is $p < 0.05$.
- (J-K)** Bubble plot showing total mass (x-axis) and total molecular number (bubble size) of cellular compartments (y-axis) in healthy (green colour) and diseased genotypes (other colours). J shows main cellular compartments while K shows the neutrophil granule subsets.

- (L) Hydrophobicity scores (y-axis) using amino acid hydrophobicity values of the last 9 n-terminal amino acids. Inclusion criteria per genotype (vs healthy donor, x-axis) was $\text{adj.p} < 0.05$ and $\text{abs}(F_c) > 1$. Each dot represents a protein, the violin plot shows the distribution of proteins with equal scores.

Figure 4. Maturation, processing and targeting of newly identified SRP dependent proteins (de novo expression).

- (A)-(D) Immunoblot analysis of HeLa cell lysates expressing tetracycline-induced PRL-GFP, GUSB-GFP, PTX-GFP and CRISP-GFP. Cells were treated with control or SRP siRNAs and processed for immunoblotting with the indicated antibodies. Experiment performed in triplicate.
- (E) Confocal microscopy images of HeLa cells depleted of endogenous SRP proteins by siRNA and stably expressing PTX3-GFP. Cells were immunostained with an anti-Calnexin antibody and DNA was visualized with DAPI. Scale bar, 10 μm . Experiment performed in triplicate.
- (F) Confocal images of HeLa cells depleted of endogenous SRPs by siRNA and stably expressing CRISP3-GFP. Cells were immunostained with an anti-GM130 antibody and DNA was visualized with DAPI. Scale bar, 10 μm . Experiment performed in triplicate.
- (G) Quantification of the co-localization of CRISP3-GFP with GM130. (unpaired t test, two-tailed ($P < 0.0001$ and $P < 0.005$)). Quantitative analysis represents 3 independent experiments.

Figure 5. Expression and localization of CRISP3 in iPSC-derived neutrophil-like granulocytes and in primary cells.

- (A) Immunoblot analysis of lysates from iPSC-derived control and SRP-mutated iPSC cells harvested at differentiation day 26. Cells were harvested at day 26, lysed and processed for immunoblotting with the indicated antibodies.
- (B) Confocal images of iPSC-derived control and SRP-mutated cells stained for CRISP3. Cells were immunostained at differentiation day 26 with an anti-CRISP3 antibody and DNA was visualized with DAPI. Scale bar, 10 μ m.
- (C) Confocal images of immunostaining of CRISP3 in a healthy donor (HD) and in a patient with the identified SRP19 gene variant. DNA was visualized with DAPI. Scale bar, 10 μ m. The experiment in (A) and (B) was performed in triplicate, the experiment in (C) twice.

Figure 6. Zebrafish models of SRP component loss-of-function effects on neutrophil abundance.

- (A) Schematic of global CRISPR/Cas9 *srpra* knockdown in zebrafish by microinjection of *srpra* gRNA and Cas9 into 1-cell embryos.
- (B) Impaired survival of global *srpra* crisprant embryos at 3 dpf compared with control non-injected siblings (n=3 independent experiments; total embryos in each experiment (n control / n crisprant): 179/127, 195/184, 133/113). Unpaired 2-tailed t-test.
- (C) Representative dysmorphic surviving *srpra* *Tg(mpx:EGFP)* crisprant embryo at 5 dpf. Panels show (i) bright field, (ii) rhodamine dextran (tracing reagent delivery) and (iii) EGFP (neutrophil reporter gene) images.
- (D) Sanger sequencing chromatogram confirming on-target *srpa* gene editing in global crisprants. (i) WT sequence from non-injected control. (ii) Sequence from severely deformed dead embryo, showing multiple superimposed

heterogeneous traces starting in the vicinity of the gRNA-targeted PAM site (red line).

- (E) Schematic of neutrophil-specific CRISPR/Cas9 *srpra* knockdown in zebrafish by microinjection of synthetic *srpra* gRNA into 1-cell *mpx-cas9* zebrafish embryos.
- (F) Depleted trunk neutrophil numbers in *mpx-cas9* embryos with neutrophil-specific *srpra* gene knockdown (pooled embryos from n=2 experiments, indicated by different colour symbols). Unpaired 2-tailed t-test.
- (G) Representative images corresponding to the two groups in (F). White box shows area where trunk neutrophil numbers were enumerated.
- (H) Sanger sequencing chromatogram confirming on-target *srpa* gene editing in neutrophils of *mpx-cas9* neutrophil-lineage crispants. (i) WT reference sequence from non-injected control. (ii) Sequence from DNA prepared from neutrophils of *mpx-cas9* neutrophil-lineage crispants, showing sequence heterogeneity starting in the vicinity of the PAM site (red line).
- (I) Schematic of global *srpr19* knockdown in zebrafish by microinjection of *srpra* splice-blocking morpholino into 1-cell *Tg(mpx:EGFP)* zebrafish embryos.
- (J) Trunk neutrophil numbers in *srp19*-MO injected morphants scored at 2 dpf (n=24-53 embryos/group; Experiment 1). 1-way ANOVA with Dunnett's post hoc test. Corresponding embryo survival rates in supplementary Figure 9E.
- (K) Trunk neutrophil numbers in *srp19*-MO injected morphants scored at 3 dpf (n=24 embryos/group; Experiment 2). 1-way ANOVA with Dunnett's post hoc test. Corresponding embryo survival rates in supplementary Figure 9F.

